

A ketone-functionalized Zn-MOF for solvent-free cyanosilylation of aldehyde and treatment activity against osteosarcoma trough increasing Mg63 cells autophagy

Tao Peng , Peng Jia , Rui Wang , Haoyu Feng & Xiao-Ming Han

To cite this article: Tao Peng , Peng Jia , Rui Wang , Haoyu Feng & Xiao-Ming Han (2020): A ketone-functionalized Zn-MOF for solvent-free cyanosilylation of aldehyde and treatment activity against osteosarcoma trough increasing Mg63 cells autophagy, Journal of Coordination Chemistry, DOI: [10.1080/00958972.2020.1819538](https://doi.org/10.1080/00958972.2020.1819538)

To link to this article: <https://doi.org/10.1080/00958972.2020.1819538>

 View supplementary material 

 Published online: 23 Sep 2020.

 Submit your article to this journal 

 View related articles 

 View Crossmark data 



A ketone-functionalized Zn-MOF for solvent-free cyanosilylation of aldehyde and treatment activity against osteosarcoma through increasing Mg63 cells autophagy

Tao Peng^a, Peng Jia^a, Rui Wang^b, Haoyu Feng^b and Xiao-Ming Han^a

^aDepartment of Orthopedics, Shandong Provincial ENT Hospital, Shandong Provincial ENT Hospital Affiliated to Shandong University, Jinan, Shandong, China; ^bDepartment of Medicine, Shanxi Hospital, Taiyuan, Shanxi, China

ABSTRACT

In this work, 5,5'-carbonyldiisophthalic acid (H₄cipa) was used as a ligand to react with Zn(NO₃)₂·6H₂O in a mixed solvent of DMF and water to prepare a new metal-organic framework (MOF) with the chemical formula of [Zn₂(cipa)(H₂O)₂](DMF) (1). Due to its O donor sites within the one-dimensional channels and high density of open metal sites, the activated **1a** was applied as a heterogeneous catalyst for the formation of C–C bonds of carbonyl compounds in the absence of solvents, which shows high efficiency and size-selectivity. Furthermore, the possible reaction mechanism has been proposed based on the experimental results. The treatment activity of the new compound on the Mg63 osteosarcoma cell line was evaluated and the possible mechanism was discussed. First, flow cytometry was performed to detect the levels of the Mg63 cancer cells' autophagy levels after indicated compound treatment. Next, real time RT-PCR assay was further conducted to measure the relative expression levels of the autophagic genes under treatment.

ARTICLE HISTORY

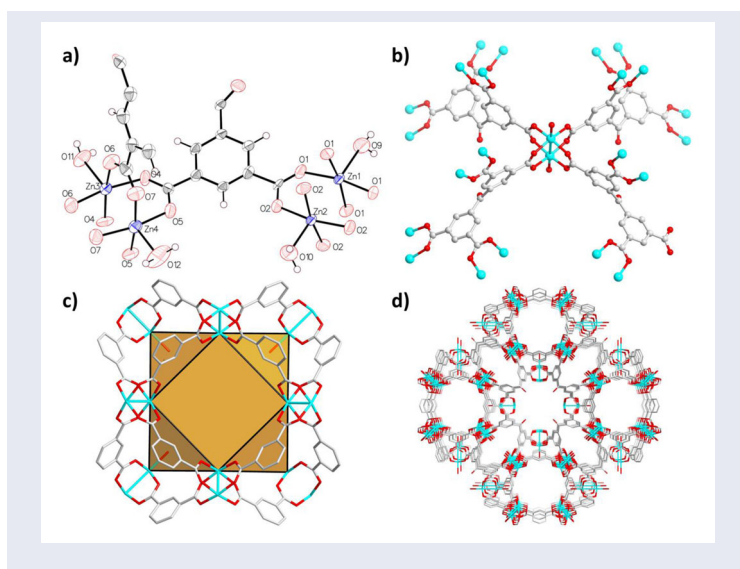
Received 21 April 2020
Accepted 16 August 2020

KEYWORDS

Zn(II)-framework; porous structure; nano-cages; cyanosilylation reaction; osteosarcoma

CONTACT Xiao-Ming Han h_xiaoming11@126.com Department of Orthopedics, Shandong Provincial ENT Hospital, Shandong Provincial ENT Hospital Affiliated to Shandong University, Jinan, Shandong, China

Supplemental data for this article is available online at <https://doi.org/10.1080/00958972.2020.1819538>.



1. Introduction

Osteosarcoma, also known as osteogenic sarcoma or osteosarcoma, is one of the most common primary malignant tumors of bone. Osteosarcoma is highly malignant and develops rapidly, and often occurs in lung metastases [1]. The incidence of osteosarcoma accounts for the highest percentage of all malignant bone tumors (44.6%), accounting for 15.5% of primary bone tumors, about 3 times that of chondrosarcoma and 7 times that of fibrosarcoma. There are more men than women with osteosarcoma, and the ratio of men to women is 2.3: 1 [2]. The age of onset is 4 to 60 years old, with 15 to 25 years old being the most common, accounting for more than 3/4. A recent study found that multiple mechanisms can regulate the process of cellular autophagy [3]. The autophagy signaling pathway has attracted wide attention from researchers.

Cyanohydrins have a significant function within biology and chemistry. They are extensively used as multi-functional components of fine chemicals, agricultural chemicals and drugs, such as β -amino alcohols, α -hydroxy acids, *etc.* [4–6]. Generally speaking, adding cyanide into carbonyl compounds is one of the basic methods to prepare them, and it is often at the synthetic chemistry forefront. In the last few decades, multiple accelerators or activators have been reported for the conversion. Under pressure to develop environment-friendly processes, organic catalysts have developed rapidly within the cyanation of carbonyl compounds catalyzed by trimethylsilyl cyanide (TMSCN) [7–9]. Metal-organic frameworks (MOFs) are novel materials, which were formed through the coordination of metal clusters and organic ligands. MOFs have many unique properties, such as high porosity, large specific surface area, and adjustable pore size as well as various functions, which make them heterogeneous catalysts with shape- and size-selectivity [10–13]. Recent literature has revealed that MOFs with coordinatively unsaturated Zn(II) metal sites are promising

candidates for the cyanosilylation reactions. For instance, Bharadwaj and coworkers reported a Zn(II)-MOF with water bound metal centers, which could act as an effective catalyst for cyanosilylation reactions and Knoevenagel condensations with size selective performance [14]. Recycling experiments showed that this Zn(II)-MOF could be reused at least five times without any loss of activity. Gu *et al.* obtained a DABCO-functionalized Zn-MOF with one-dimensional channels, which could behave as a size selective catalyst for the cyanosilylation reaction [8]. Yuan's group constructed a Zn(II)-MOF with coordinatively unsaturated metal sites using a pyridyl-tricarboxylate ligand, which can be used as a highly efficient size selective heterogeneous catalyst for the solvent-free cyanosilylation of acetaldehydes under mild conditions [15]. Based on the above results from the literature, both the open metal sites and the open O donor sites could act as the binding sites for the cyanosilylation reaction. In this work, 5,5'-carbonyldiisophthalic acid (H_4cipa) was used as a ligand to react with $Zn(NO_3)_2 \cdot 6H_2O$ in a mixed solvent of DMF and water to prepare a new metal-organic framework (MOF) with the chemical formula of $[Zn_2(cipa)(H_2O)_2](DMF)$ (**1**). Due to its O donor sites within the one-dimensional channels and high density of open metal sites, the activated **1a** was applied as a heterogeneous catalyst for the formation of C–C bonds of carbonyl compounds in the absence of solvents, which shows high efficiency and size-selectivity. Furthermore, the possible reaction mechanism has been proposed based on the experimental results. Through biological functional study, the treatment activity of the compound on the Mg63 osteosarcoma cell line was evaluated *in vitro*, and the related mechanism was explored at the same time. The results of the flow cytometry indicated that the compound could significantly reduce the autophagy levels in the Mg63 osteosarcoma cells. In addition to this, the data of the real time RT-PCR also suggested that the relative expression levels of the autophagic genes were promoted by the compound exposure.

2. Experimental

2.1. Chemicals and measurements

$Zn(NO_3)_2 \cdot 6H_2O$ (AR) was purchased from Beijing Beihua Chemicals Co., Ltd. 5,5'-Carbonyldiisophthalic acid (97%) was obtained from Shanghai Guoyao Chemicals Co., Ltd. TMSCN and various aldehydes used in the catalytic reaction were bought from Beijing Bailingwei Technology Co., Ltd. The solvents used in this research were purchased from Tianjin Guangfu Chemicals Co., Ltd. With the Nicolet Avatar 360 FT-IR spectrophotometer we determined FT-IR spectra. The heat analysis equipment of Q50 TGA (TA) was utilized for the analysis of thermogravimetry under nitrogen flow; the heating rate was $5^\circ C \cdot min^{-1}$. On a MiniFlex (Cu $K\alpha$, $\lambda = 1.5418 \text{ \AA}$) we determined bulk samples' powder X-ray diffraction (PXRD) at room temperature. The gas chromatography analysis was performed with an Agilent 7890B gas chromatograph. The isotherms of gas adsorption (N_2) at low pressure (up to 1 bar) were determined using a Micrometrics ASAP 2020 porosity analyzer along with specific surface area.

Table 1. Crystallographic parameters along with refinement details for **1**.

Empirical formula	C ₁₇ H ₁₀ O ₁₁ Zn ₂
Formula weight	1562.97
Temperature/K	150.15
Crystal system	tetragonal
Space group	I4/mmm
a/Å	30.461(2)
b/Å	30.461(2)
c/Å	23.0136(13)
α/°	90
β/°	90
γ/°	90
Volume/Å ³	21354(3)
Z	8
ρ _{calc} /cm ³	0.982
μ/mm ⁻¹	1.381
Reflections collected	71114
Independent reflections	5161 [R _{int} = 0.1100, R _{sigma} = 0.0832]
Data / restraints / parameters	5161 / 3 / 226
Goodness-of-fit on F ²	1.053
Final R indexes [I >= 2σ (I)]	R ₁ = 0.0688, ωR ₂ = 0.1852
Final R indexes [all data]	R ₁ = 0.0882, ωR ₂ = 0.1977
Largest diff. peak / hole / e Å ⁻³	1.31 / -0.64
CCDC	1968357

2.2. Preparation and characterization for catena-[(μ-5,5'-carbonylbis(benzene-1,3-dicarboxylato))-bis-aqua-bis-zinc(II) dimethylformamide] (**1**) and catena-[(μ-5,5'-carbonylbis(benzene-1,3-dicarboxylato))-bis-zinc(II)] (**1a**)

A mixture of H₄cipa of 10 mg and 0.028 mmol along with Zn(NO₃)₂·6H₂O, which was 20 mg and 0.083 mmol, were mixed with HBF₄ (50% in H₂O, 0.6 mL) and DMF (2.0 mL). The mixture was transferred to a vial with a screw cap, which was sealed and heated in the oven for three days at 90 °C. Colorless single crystals with block-shape were collected and then washed using DMF several times to obtain **1** and the yield was 8 mg (52% on the basis of ligand H₄cipa). Anal. Calcd for **1** (C₂₀H₁₇NO₁₂Zn₂): C, 40.43; H, 2.88; N, 2.36%. Found for **1**: C, 40.23; H, 2.77; N, 2.54%. Main FT-IR absorptions (KBr pellets, cm⁻¹): 3382, 2973, 1646, 1447, 1378, 1286, 1044, 734.

The solvent-free samples of **1** (denoted as **1a**) were prepared using the following procedure: 200 mg of **1** was soaked in MeOH (20 mL) for three days, during which fresh MeOH was replaced every 12 h. Then the solvent-exchanged samples were added into an adsorption test tube and heated at 110 °C for one day under a dynamic vacuum.

Applying an Oxford Xcalibur E diffractometer we acquired compound **1**'s X-ray data using the software CrysAlisPro to analyze strength data and then convert it into HKL files [16]. Empirical absorption correction was applied using spherical harmonics, implemented in SCALE3 ABSPACK scaling algorithm [17]. Complex **1**'s starting structure pattern was established by the program of Olex2.solve embedded in the OLEX2 software and modified via the program SHELXL-2014 according to the least square method [18,19]. Complex **1**'s non-H atoms were refined with anisotropic parameters; hydrogens were fixed to their linked C atoms using AFIX commands. Due to the highly disordered nature of the lattice DMF molecule, it could not be refined, so its electronic

contribution was removed via the SQUEEZE manipulation embedded in the PLATON software. The detailed analysis of the SQUEEZE results is discussed in the Supporting Information. The final chemical formula of **1** was determined via a combination of the results from the single crystal X-ray diffraction, elemental analysis and the TGA data [20]. Table 1 describes compound **1**'s crystal.

2.3. The heterogeneous catalytic cyanosilylation with **1a**

Dried Zn(II)-MOF catalyst (0.005 mmol) was added to a mixture of the corresponding carbonyl compound (0.5 mmol) and trimethylsilyl cyanide (0.133 mL, 1.0 mmol) under nitrogen atmosphere. Then, the mixture was stirred at 40 °C. The reaction was monitored by GC (FID from AGILENT 7820) using a cross-linked (95%)-dimethyl-(5%)-diphenylpolysiloxane column (HP-5, 30 m × 0.32 mm × 0.25 μm), helium, injector temperature 250 °C, detector temperature 300 °C, and oven temperature program 45 °C (3 min)–20 °C·min⁻¹–280 °C (2 min). The reaction conversions were determined by gas chromatography (GC) analysis. For filtration tests, the catalyst was separated after a reaction time of 2 h with 50% conversion. The reaction was allowed to proceed in the filtrate, with no additional conversion after 17 h.

2.4. Cell counting kit-8

To determine the inhibitory effect of the synthetic compound on the viability of the Mg63 osteosarcoma cell, the CCK-8 assay was performed. All operations were carried out under the guidance of the instructions with some modifications. In brief, the Mg63 osteosarcoma cells were used for the indicated evaluations. Mg63 cells used in this research were purchased from ATCC and cultured in DMEM culture medium with the penicillin-streptomycin solution. After growth into the logical growth phase, the cells were collected and seeded into the 96 well plates at the final density of 10⁴ cells per well. The plates were then placed in an incubator at 37 °C, 5%CO₂. Then the cells were exposed to the compound at a series concentration (1, 2, 4, 8, 10, 20, 40, 80 μM). The cells were incubated for a further 48 h, and the cell supernatant was discarded. Fresh medium was added containing 10% CCK-8 solution. Finally, the absorbance of each well was measured with a spectrophotometer at 490 nm. This experiment was repeated at least three times, and the results were presented with mean ± SD.

2.5. Flow cytometry

The flow cytometry was performed in this research to detect the influence of the compound on the Mg63 osteosarcoma cell autophagy. Before the experiment, the Mg63 osteosarcoma cells were first transfected with LC3-GFP plasmid, and then the following protocols were performed according to the instructions as previously described. Mg63 cells harboring the LC3-GFP plasmid in the logarithmic growth phase were collected and inoculated into 6 well plates and the density of 1 × 10⁵ cells per well. After incubation in an incubator for 12 h, the compound was added into the wells at concentrations of 5 μM and 10 μM. The ligand and metal ion were used for the control

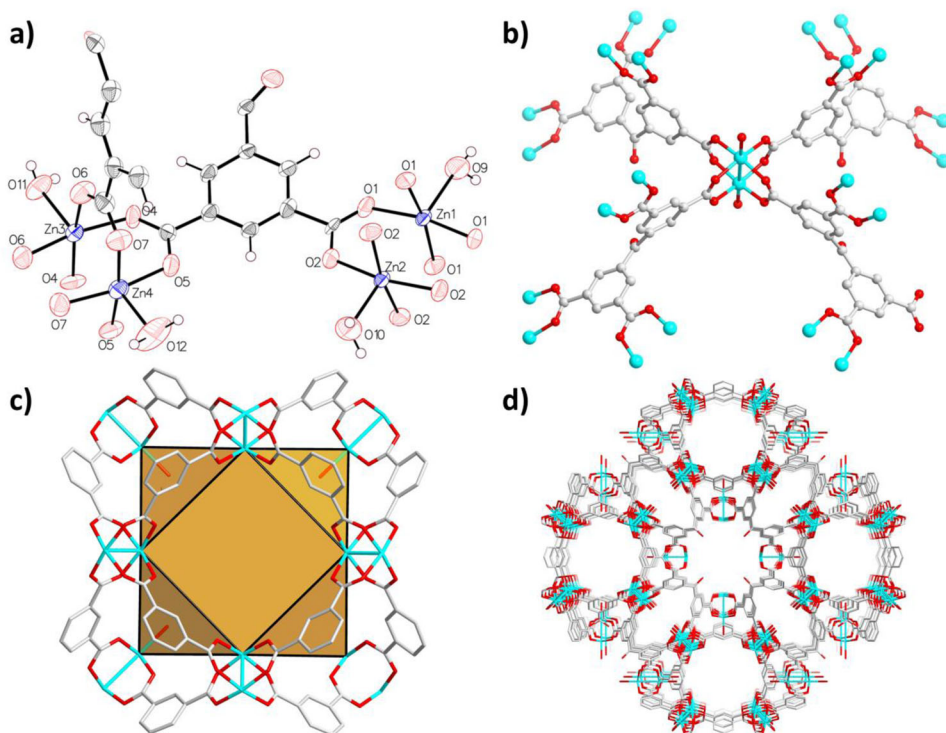


Figure 1. (a) View for the asymmetric unit for 1. (b) A view of the organic ligand coordination mode. (c) The rhombicuboctahedral cage in 1. (d) A perspective view for the channels along with cages formed within the three-dimensional skeleton.

treatments. PBS and cell apoptosis inducer were used as negative and positive control. In the end, the cells in the different groups were harvested and then washed with PBS three times. The fluorescence absorption value was measured with flow cytometry. The experiment was repeated for three or more times.

2.6. Real time RT-PCR

Real time RT-PCR was further conducted to demonstrate the induction effect of the compound on the Mg63 cell line autophagy levels by measuring the relative expression of the autophagic *atg5* and *atg7* genes. This experiment was finished in accordance with the instructions with some modifications. Briefly, the Mg63 cancer cells within the phase of logarithmic growth were collected and inoculated into 96 well plates at the ultimate density 1×10^5 cells/well. After 12 h culturation at 37°C , $5\%\text{CO}_2$ environment, the cells were then treated with the compound at the concentration of $5\ \mu\text{M}$ and $10\ \mu\text{M}$ using the ligand and metal ion as the control treatment. After compound treatment, the Mg63 cancer cells were collected and washed with PBS 3 times, then the TRIzol Reagent (Sigma, St. Louis, MO, USA) was used to extract total RNA in the cells. The quality and quantity of the extracted RNA was measured and then reversely transcribed into cDNA using an RNA reverse transcription kit according to protocols. In the end, the relative expression level of the *atg5* and *atg7* gene in the

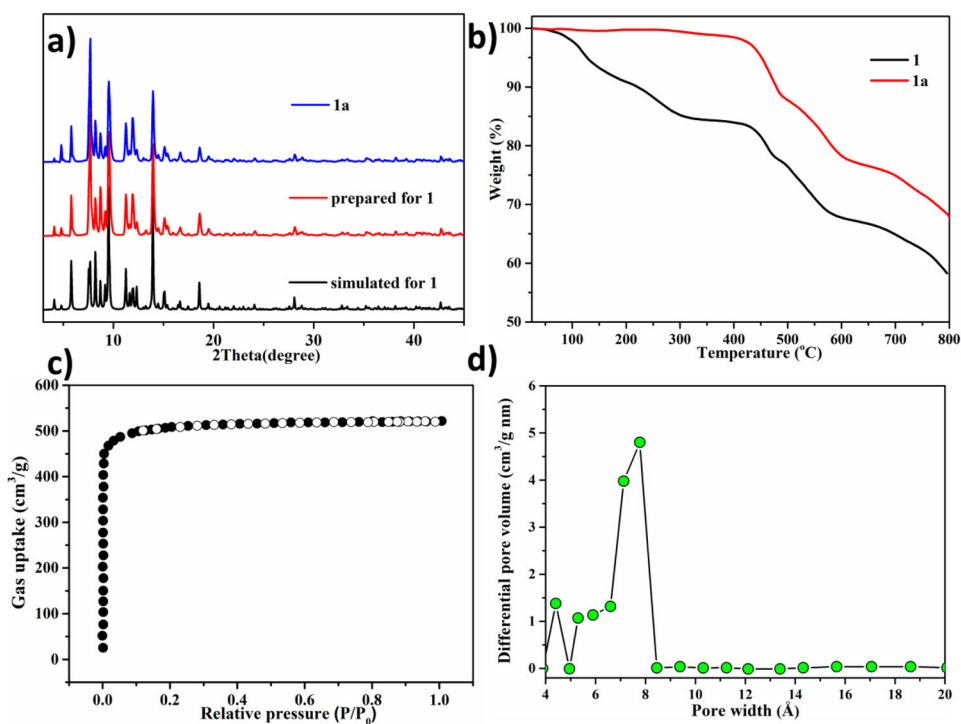


Figure 2. (a) **1a**'s and **1**'s pattern of PXRD. (b) **1a**'s and **1**'s curves of TGA. (c) **1a**'s N₂ adsorption data at 77 K. (d) Calculating **1a**'s distribution of pore size by Horvath–Kawazoe approach.

Mg63 cancer cells was measured with real-time RT-PCR. This experiment was performed in triplicate and analyzed utilizing the $2^{-\Delta\Delta C_t}$ approach.

3. Results and discussion

3.1. Crystal structure of **1**

According to the results of elemental analysis and single-crystal X-ray diffraction as well as thermogravimetry, in water along with DMF mixed solvent, Zn(NO₃)₂·6H₂O reacts with H₄cipa after 48 h to form colorless crystals of [Zn₂(cipa)(H₂O)₂](DMF)₂. According to the crystal data, which were collected at ambient temperature, **1** crystallizes within the tetragonal space group I4/mmm; the unit cell parameters are $a = b = 30.461(2)$ Å and $c = 18.6322(14)$ Å. The unit cell volume is 21354(2) Å³. **1**'s basic molecular repeating unit contains four crystallography independently Zn(II) ions, one and a quarter fully deprotonated cipa²⁻ ligands and four coordinated water molecules (Figure 1(a)). The crystallographic analysis shows that **1** has a three-dimensional structure composed of organic cdip⁴⁻ connectors along with binuclear propeller Zn₂(COO)₄ secondary building units (SBU). Within each binuclear SBU, every Zn(II) ion coordination geometry is regarded as a five-coordinate pyramid and the τ value is 0, which is formed via four oxygen carboxylic acid oxygen atoms of four distinct cipa²⁻ ligands along with a coordinated water molecule. The length of the zinc-oxygen bonds at the apex [2.114(9)–2.146(8) Å] were obviously longer than the 4 zinc-oxygen bond lengths

Table 2. Optimization of conditions for the cyanosilylation reaction.

Entry	Cat. mol %	TMSCN	Temp. (°C)	Conv. (%) ^a
1	0	3 eq	rt	40
2	2	3 eq	rt	76
3	2	3 eq	40	98
4	1	3 eq	40	98
5	0.5	3 eq	40	84
6	1	2 eq	40	96
7	1 (reused 1a)	2 eq	40	94
8	1 (Zn(NO ₃) ₂ ·6H ₂ O)	2 eq	40	66
9	2 (Zn(NO ₃) ₂ ·6H ₂ O)	2 eq	40	75

^aDetermined via GC on the basis of carbonyl substrate.

on the base [1.947(3)–1.938(4) Å]. The Zn(II)-O bond distances are comparable with those observed in other MOFs based on the Zn₂(COO)₄ cluster such as [Zn₇(TMBHB)₂·2NO₃·5DMF·4CH₃CH₂OH·6H₂O]_n (Zn(II)-O bond distance: 1.984(10)–2.146(18) Å) [21], [Zn₂(dbda)(H₂O)₂] (Zn(II)-O bond distance: 2.004(11)–2.149(10) Å) [22]. The Zn-Zn separations are between 2.6461(17) and 2.6514(11) Å, which are similar to the reported within other MOFs based on Zn(II) with SBUs of Zn₂(COO)₄ [21–23]. It is found that the organic cdip⁴⁻ unit has two configurations, and the two benzene rings have distinct dihedral angles [62.3(5) and 75.8(5)°] along with ketone-related C–C–C bond angles [114.3(5) and 101.1(5)°] (Figure 1(b)). In general, **1**'s structural porosity is chiefly because of peripheral channels between the cages and the formation of rhombic octahedral cage (Figure 1(c)). In each rhombic octahedral cage, there are eight triangular windows along with six quadrilateral windows. The former has a radius of 2.0 Å and the latter is 3.8 Å, neglecting the atoms' van der Waals radii of. The channels on the periphery are modified via non-coordinative polar carbonyl functions with ~2.5 Å radius. This shows that the porosity could provide favorable conditions for gas entry. Using Platon's SOLV function, **1**'s total accessible volume of solvent was calculated as 14081 Å³, accounting for about 65.9% of the total structure volume (Figure 1(d)). The structure of **1** is isostructural to the Cu(II)-MOF based on the same ligand [24].

3.2. Pxd, TGA analysis and gas sorption properties

By measuring the newly prepared samples at room temperature, **1**'s phase purity was determined via powder X-ray diffraction (PXRD). The solvated samples PXRD diagram was consistent with that of the simulated samples in crystal data, revealing that the prepared samples had high phase purity (Figure 2(a)). The newly prepared **1**'s thermogravimetric analysis shows that the weight loss was about 17.83% between 75 °C and 253 °C, equivalent to the removal of one lattice DMF and two coordinated water molecules (calcd: 18.35%) (Figure 2(b)). Above 450 °C, the second weight loss could be observed, indicating decomposition of the organic ligand and the collapse of the whole framework. The final product is ZnO (JCPDS card no. 36-1451). Furthermore, the samples were immersed in methanol for solvent exchange and then heated under a dynamic vacuum at 110 °C for one day to carry out **1**'s desolvation. PXRD analysis of the completely desolvated skeleton reveals that the crystallinity of the porous material still remained. The absence of coordinated and lattice solvents has been confirmed via

Table 3. The cyanosilylation reaction of different aldehydes in the existence of **1a**.

Entry ^a	R ₁	R ₂	Conv.(%) ^b
1	Ph	H	96
2	4-CH ₃ C ₆ H ₄	H	94
3	2-CH ₃ C ₆ H ₄	H	88
4	4-ClC ₆ H ₄	H	99
5	1-Naphthyl	H	78
6	9-Anthryl	H	66
7	2-Furyl	H	0
8	n-Bu	H	99
9	(CH ₂) ₅	H	99

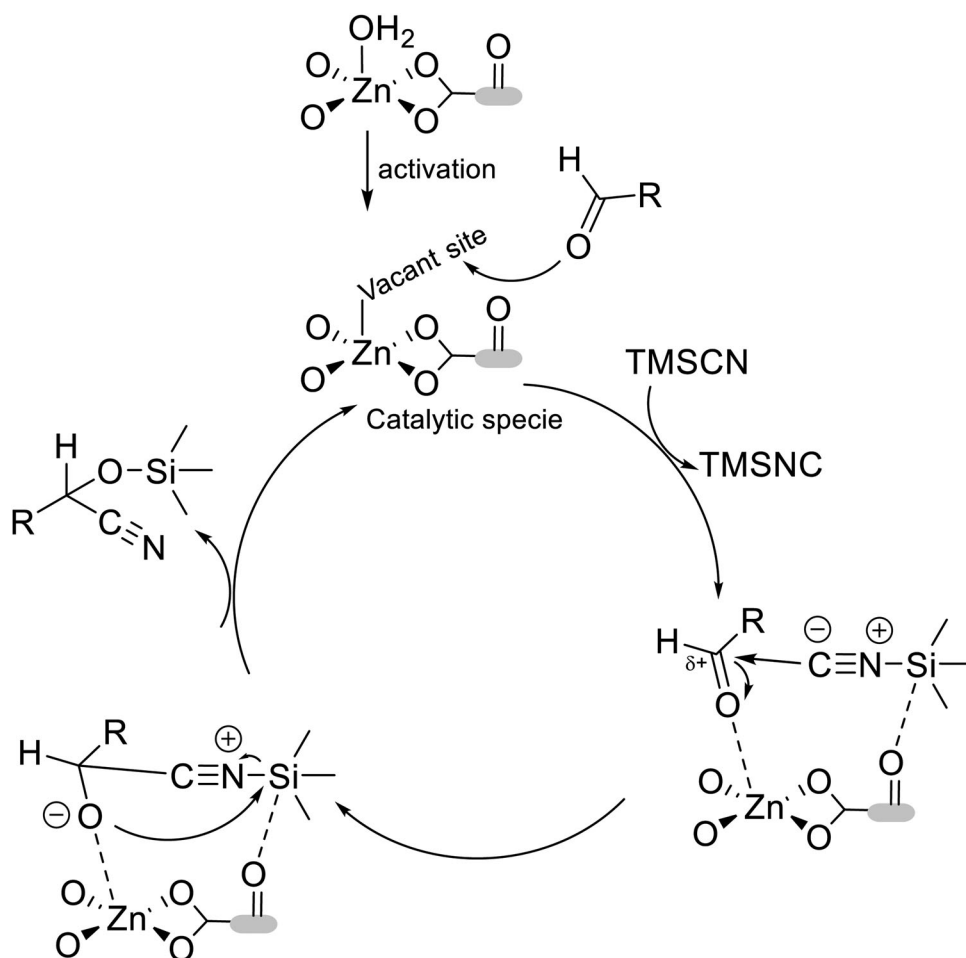
^aThe reaction conditions are Me₃SiCN (1 mmol), 0.5 mmol of aldehyde/ketone, and **1a** (0.013 mg, 0.005 mmol) at 40 °C and under N₂.

^bDetermined via GC on the basis of carbonyl substrate.

the TGA curve of **1a** as shown in Figure 2(b). The activated **1a**'s permanent porosity was demonstrated via the measurements of gas adsorption. According to Figure 2(c), **1a** shows a typical type I adsorption behavior. At 1 bar and 77 K, the saturated absorption of N₂ is 522.1 cm³·g⁻¹. According to the adsorption of N₂ at 77 K, the Brunauer-Emmett-Teller and Langmuir surface areas are 1539 and 2259 m²·g⁻¹, respectively. **1a**'s pore volume is 0.81 cm³·g⁻¹. N₂ isotherms' distribution of pore size at 77 K was analyzed via the Horvath-Kawazoe approach. It was found that Cu-MOF **1**'s distribution of pore size is about 7.6 Å, which is close to the distribution seen in the single-crystal structure. This characteristic clearly shows **1**'s microporous nature (Figure 2(d)).

3.3. Catalytic properties of **1a**

In order to compare **1a**'s catalytic activity with other MOFs, we examined carbonyl compound's cyanation. After removing the coordination water molecules, the strong acid, unsaturated metal centers of **1a**'s pores volume increases. First, the model experiment was carried out using benzaldehyde as a standard molecule and changing the amount and temperature of catalyst without solvent. We are pleased that, according to Table 2, the conversion of benzaldehyde in a nitrogen atmosphere at 40 °C was 96% with a **1a** loading of 1 mol%, which is only one-eleventh of the conversion observed in the relevant Mn-BTT reported [25]. In contrast, we found that our catalyst's activity was higher than the activity of some formerly reported catalysts (Ln-MOFs along with Sc-MOF), in which the catalyst loading was 5 mol% [26,27]. **1a** is removed via filtration after 2 h reaction stops, providing only 51% of the total conversion after 15 h. This shows that there is no homogeneous catalyst species within the reaction solution, and **1a** is indeed heterogeneous in nature. To study the important roles of the open metal sites as well as the formation of a porous framework for **1a** in the catalytic reaction, a comparison experiment was carried out using the equivalent amount of Zn(NO₃)₂·6H₂O as the catalyst, which gave a yield of only 66% under the same reaction conditions after 12 h (Table 2 entry 8). Further increase of the concentration of Zn(NO₃)₂·6H₂O showed only a slight increase of the conversion (from 66% to 75%, Table 2 entry 9), and such an experimental phenomenon might be due to the enhanced Lewis acidity of the open Zn(II) sites in **1a** than that of the Zn(II) in Zn(NO₃)₂·6H₂O. More importantly, it should be pointed out that **1a** could be



Scheme 1. The suggested mechanism of **1a** catalytic reaction.

conveniently separated from the reaction system via filtration and reused for a second time after the activation at 80 °C for 12 h without losing catalytic efficiency, but the separation of $\text{Zn}(\text{NO}_3)_2 \cdot 6\text{H}_2\text{O}$ from the reaction system needs the extraction or even the silica gel column chromatography operations, without considering reusing experiments. The results from the comparison experiments highlight the important role of open metal sites as well as the open framework for **1a** in the cyanosilylation reaction.

Under the high conversion rate and high efficiency conditions, we turned our attention to the investigation of the scope of **1a** as a catalyst for general use; the results are summarized in Table 3. The results showed that the reaction had a wide tolerance to different substrates. Aryl- (Table 3, items 1-4), heteroaryl- (Table 3, item 7) and aliphatic aldehydes (Table 3, item 8) or a cyclic ketone (Table 3, item 9) were appropriate substrates and the relevant cyanohydrin trimethylsilyl ethers were produced in high to outstanding conversions. According to Table 3, neither substituent position on the aromatic ring or electronic effect revealed any obvious variety in the total conversion. Furthermore, an obvious effect of size-selectivity was discovered in **1a**; when the

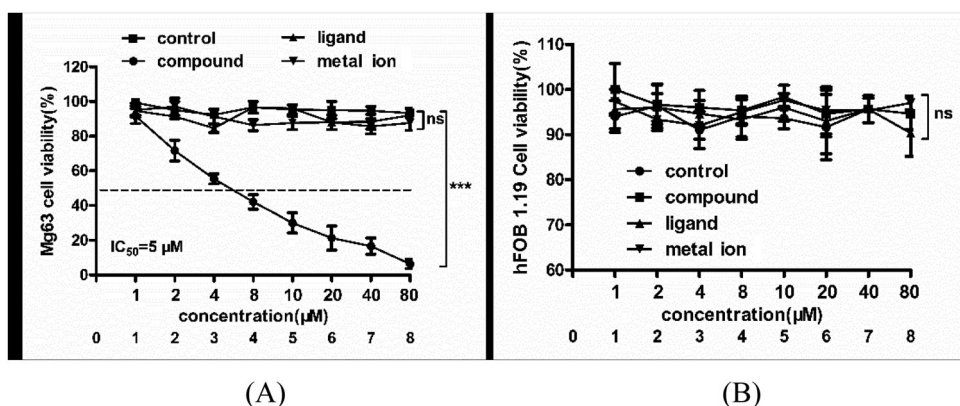


Figure 3. Inhibited viability of the Mg63 cancer cells after compound treatment. Mg63 cancer cells in the logical growth phase were harvested and inoculated into 96 well plates and then treated by a series of compounds. The CCK-8 determination was performed to detect the inhibitory activity of the compound on the Mg63 cancer cells (A). The cytotoxicity of the compound on human osteoblast hFOB 1.19 (B).

substrate was 1-naphthaldehyde, only 78% product was acquired (Table 3, item 5), and 9-anthracene formaldehyde had a much lower conversion efficiency (Table 3, item 6). It also shows that cyanation takes place in MOF-**1a** pores.

According to the results of the experiments and prior reports, a reasonable reaction mechanism was put forward to explain the cyanation process of **1a** catalyst [27–33]. The unstable water molecules within **1a** channels were removed via heating at the aim of exposing the unsaturated metal centers. Activating the aldehydes occurred via coordination to unsaturated centers of zinc followed by reaction with TMSCN. Meanwhile, the TMSCN could also be stabilized by the O donor groups in the pores of **1a**. Fresh aldehydes replaced products, and the catalysts activate aldehydes continuously within the next cycle of catalysis (Scheme 1).

3.4. Compound inhibited the viability of the Mg63 cancer cells

Cancer cells are the root of tumors and the result of normal cell mutation. Different from normal cells, cancer cells have three characteristics of infinite growth, transformation and metastasis, and can proliferate infinitely and destroy normal cell tissues. Thus, in the biological functional study of this experiment, the CCK-8 preformation was first conducted to determine the inhibitory effect of the compound on the Mg63 cancer cells using the ligand and metal ion as the control treatment. As the results show in Figure 3, we can see that different from the control group, the compound could reduce the viability of the Mg63 cancer cells, and there was a significant difference between these two groups. However, both the ligand and metal ion have no effect on the cancer cell viability (A). In addition to this, the compound, as well as the ligand and ion showed no cytotoxicity against human hFOB 1.19 osteoblast (B). This result suggested that the compound has potential inhibitory activity on the cancer cells growth with low cytotoxicity.

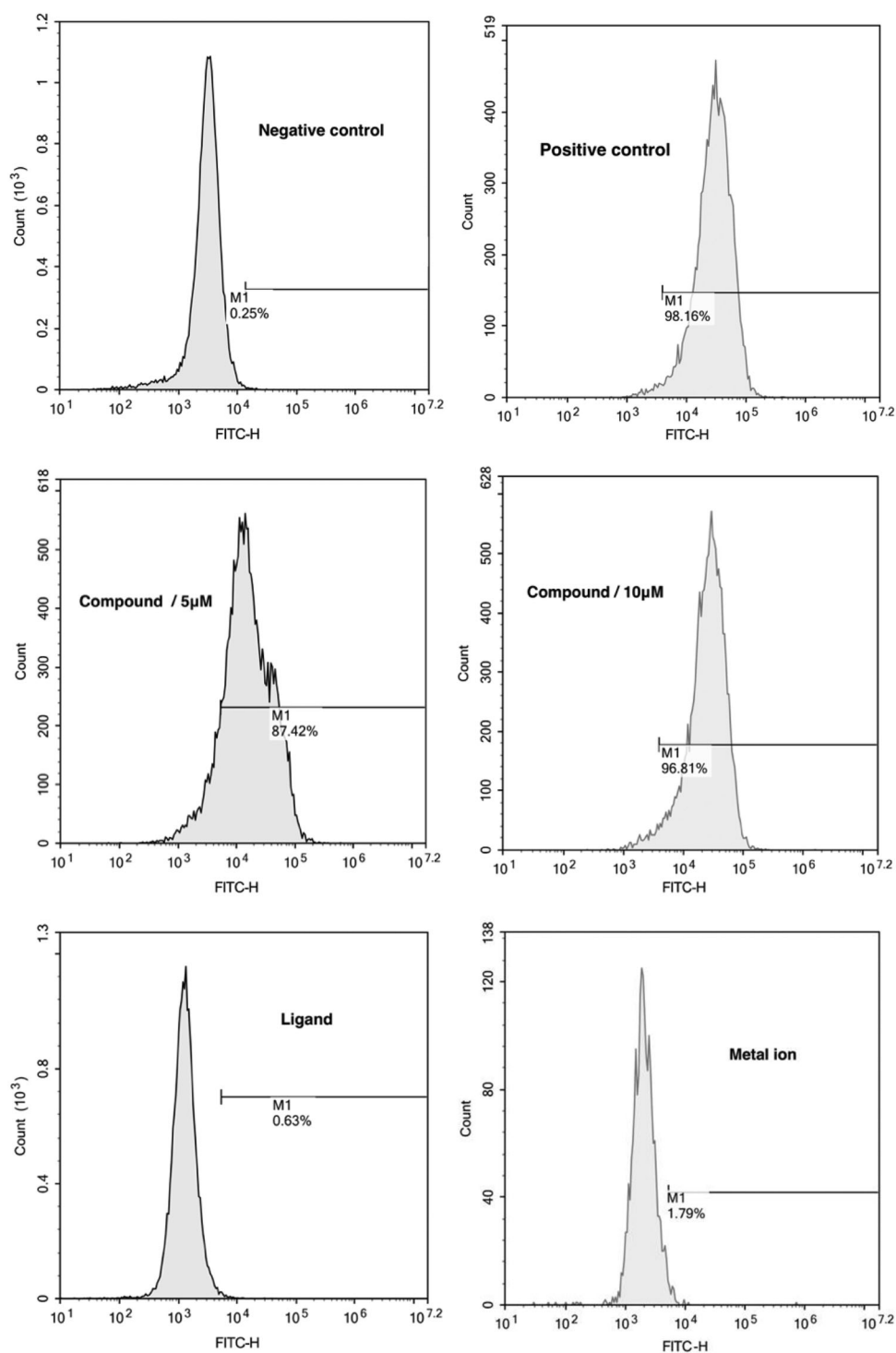


Figure 4. Increased Mg63 cells autophagy level after compound treatment. Mg63 cells were transfected with LC3-GFP plasmid, seeded into 6 well plates and then exposed to the indicated concentration of the compound. Flow cytometry was used to measure the fluorescence absorption value of different groups after compound treatment, which reflected the cancer cell autophagy levels.

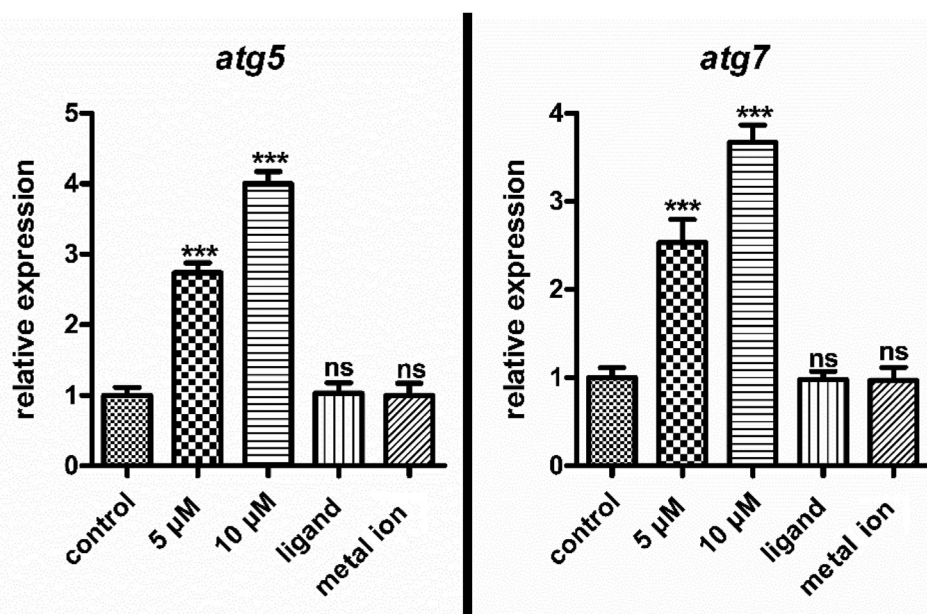


Figure 5. Induced the *atg5* and *atg7* relative expression in the Mg63 cells after compound treatment. Mg63 cancer cells in the logical growth phase were harvested and inoculated into 96 well plates and then treated by a series of compounds. RT-PCR was performed to determine the relative expression of *atg5* and *atg7* genes.

3.5. Compound increased the autophagy level in the Mg63 cell line

In the above experiment, we have confirmed the excellent anticancer activity of the compound on Mg63 cancer cells with low cytotoxicity. However, the specific mechanism of the compound against the Mg63 cancer cells was still unclear. Recent studies found that multiple mechanisms can regulate the process of cellular autophagy. The autophagy signaling pathway has attracted wide attention from researchers. Thus, in this present experiment, flow cytometry was performed to detect the autophagy levels in the Mg63 cancer cells after each indicated treatment. From the results in Figure 4, we found that the fluorescence absorption value of the Mg63 cells harboring LC3-GFP plasmid was significantly increased in the treatment compound group, indicating the compound treatment could evidently increase the Mg63 cells autophagy. The induction activity of the compound also showed a dose relationship, while the ligand and the metal ion still had no influence on the cell autophagy. This result revealed that the compound inhibits the osteosarcoma process by increasing the autophagy level in the Mg63 cancer cells.

3.6. Compound induced the *atg5* and *atg7* relative expression in the Mg63 cells

Through the flow cytometry assay, we revealed that the compound significantly increased the cancer cell autophagy levels. Whether the compound could regulate the relative expression levels of the autophagic genes in the Mg63 cancer cells was next examined. Real time RT-PCR was conducted for the *atg5* and *atg7* genes determination. The results in Figure 5 indicate that after compound treatment, the relative

expression levels of the *atg5* and *atg7* in the Mg63 cancer cells were significantly increased and showed dose relationship. This result was consistent with the previous study, suggesting the induction of the compound on Mg63 cancer cells autophagy.

4. Conclusion

We prepared a new MOF based on Zn(II) ions as nodes via utilizing the carbonylated tetracarboxylic acid ligand 5,5'-carbonyldiisophthalic acid (H_4 cipa). Single crystal X-ray diffraction studies showed that **1** has open metal sites running along one-dimensional channels of the *c*-axis. Due to its O donor sites within the one-dimensional channels and high density open metal sites, activated **1a** was applied as a solvent-free heterogeneous catalyst for the formation of C–C bonds of carbonyl compounds, which showed high efficiency and size-selectivity. Furthermore, according to the experimental results, we proposed a possible reaction mechanism. In biological research, the anticancer activity, as well as the specific mechanism of the compound on the Mg63 osteosarcoma cells, was evaluated *in vitro*. The results of the flow cytometry indicated that the compound could significantly reduce the autophagy levels in the Mg63 osteosarcoma cells. In addition, the data of the real time RT-PCR also suggested that the relative expression levels of the autophagic genes was promoted by the compound exposure. In conclusion, the compound showed an excellent inhibitory effect on the Mg63 osteosarcoma cells by stimulating the autophagy in the cells.

Acknowledgements

The research did not receive any specific funding.

Disclosure statement

The authors declare there is no conflict of interest regarding the publication of this paper.

Data availability

The data used to support the findings of this study are included within the article.

References

- [1] S. Qiu, L. Tao, Y. Zhu. *Med. Sci. Monit.*, **25**, 8190 (2019).
- [2] Y. Feng, Y. Liao, J. Zhang, J. Shen, Z. Shao, F. Hornicek, Z. Duan. *Cell Commun. Signal.*, **17**, 138 (2019).
- [3] T. Liu, L. Ling, Q. Zhang, Y. Liu, X. Guo. *Orthop. Surg.*, **11**, 826 (2019).
- [4] X. Feng, N. Guo, R. Li, H. Chen, L. Ma, Z. Li, L. Wang. *J. Solid State Chem.*, **268**, 22 (2018).
- [5] X. Feng, H. Chen, R. Li, M. Yang, S. Guo, L. Wang, Q. Liang, Z. Li. *Polyhedron*, **157**, 420 (2019).
- [6] X. Feng, Y.P. Shang, H. Zhang, R.F. Li, W.Z. Wang, D.M. Zhang, L.Y. Wang, Z.J. Li. *RSC Adv.*, **9**, 16328 (2019).
- [7] X. Cui, M.C. Xu, L.J. Zhang, R.X. Yao, X.M. Zhang. *Dalton Trans.*, **44**, 12711 (2015).
- [8] J.M. Gu, W.S. Kim, S. Huh. *Dalton Trans.*, **40**, 10826 (2011).
- [9] P. Phuengphai, S. Youngme, P. Gamez, J. Reedijk. *Dalton Trans.*, **39**, 7936 (2010).

- [10] X. Feng, R. Li, N. Guo, Y.S. Seik, W. Ng, X. Liu, L. Wang. *Inorg. Chim. Acta*, **459**, 87 (2017).
- [11] W. Liu, H. Li, H. Zhu, P. Xu. *Materials*, **13**, 1180 (2020).
- [12] Z. Wang, X. Zhang, S. Jiang, Y. Qu, D. Ou, J. Wang. *J. Alloys Compd.*, **828**, 154412 (2020).
- [13] C. Duan, Y. Yu, J. Xiao, X. Zhang, L. Li, P. Yang, J. Wu, H. Xi. *Sci. China Mater.*, **63**, 667 (2020).
- [14] S. Neogi, M.K. Sharma, P.K. Bharadwaj. *J. Mol. Catal. A. Chem.*, **299**, 1 (2009).
- [15] Y. Zhang, K. Su, M. Hao, L. Liu, Z.-B. Han, D. Yuan. *CrystEngComm.*, **20**, 6070 (2018).
- [16] CrysAlisPro. Agilent Technologies, Version 1.171.35.21 (release 20-01-2012 CrysAlis171.NET).
- [17] SCALE3 ABSPACK C A P. Agilent Technologies UK Ltd. 2013.
- [18] O.V. Dolomanov, L.J. Bourhis, R.J. Gildea, J.A.K. Howard, H. Puschmann. *J. Appl. Crystallogr.*, **42**, 339 (2009).
- [19] G.M. Sheldrick. *Acta Crystallogr. C. Struct. Chem.*, **71**, 3 (2015).
- [20] A.L. Spek. *Acta Crystallogr. C. Struct. Chem.*, **71**, 9 (2015).
- [21] X. Zhao, X. Wang, S. Wang, J. Dou, P. Cui, Z. Chen, D. Sun, X. Wang, D. Sun. *Cryst. Growth Des.*, **12**, 2736 (2012).
- [22] X. Zhang, Z. Zhang, J. Boissonnault, S.M. Cohen. *Chem. Commun. (Camb.)*, **52**, 8585 (2016).
- [23] D.M. Chen, X.J. Zhang. *CrystEngComm.*, **21**, 4696 (2019).
- [24] G. Feng, Y. Peng, W. Liu, F. Chang, Y. Dai, W. Huang. *Inorg. Chem.*, **56**, 2363 (2017).
- [25] S. Horike, M. Dinca, K. Tamaki, J.R. Long. *J. Am. Chem. Soc.*, **130**, 5854 (2008).
- [26] R.F. D'Vries, V.A. de la Peña-O'Shea, N. Snejko, M. Iglesias, E. Gutiérrez-Puebla, M.A. Monge. *J. Am. Chem. Soc.*, **135**, 5782 (2013).
- [27] R.F. D'Vries, M. Iglesias, N. Snejko, E. Gutiérrez-Puebla, M.A. Monge. *Inorg. Chem.*, **51**, 11349 (2012).
- [28] Z. Zhang, J. Chen, Z. Bao, G. Chang, H. Xing, Q. Ren. *RSC Adv.*, **5**, 79355 (2015).
- [29] C. Zhu, Q. Xia, X. Chen, Y. Liu, X. Du, Y. Cui. *ACS Catal.*, **6**, 7590 (2016).
- [30] A. Karmakar, A. Paul, G.M.D.M. Rúbio, M.F.C. Guedes da Silva, A.J.L. Pombeiro. *Eur. J. Inorg. Chem.*, **2016**, 5557 (2016).
- [31] L.M. Aguirre-Díaz, M. Iglesias, N. Snejko, E. Gutiérrez-Puebla, M.Á. Monge. *CrystEngComm.*, **15**, 9562 (2013).
- [32] A. de Oliveira, A. Mavrandonakis, G.F. de Lima, H.A. De Abreu. *ChemistrySelect.*, **2**, 7813 (2017).
- [33] J. Tao, Y. Guo, S. Li. *J. Mol. Struct. Theochem.*, **899**, 61(2009).